Smart agile lens remote optical sensor for three-dimensional object shape measurements

Nabeel A. Riza* and Syed Azer Reza

Photonic Information Processing Systems Laboratory, CREOL, The College of Optics and Photonics, University of Central Florida, 4000 Central Florida Boulevard, Orlando, Florida 32816-2700, USA

*Corresponding author: riza@creol.ucf.edu

Received 25 November 2009; revised 19 January 2010; accepted 22 January 2010; posted 25 January 2010 (Doc. ID 120503); published 24 February 2010

We demonstrate what is, to the best of our knowledge, the first electronically controlled variable focus lens (ECVFL)-based sensor for remote object shape sensing. Using a target illuminating laser, the axial depths of the shape features on a given object are measured by observing the intensity profile of the optical beam falling on the object surface and tuning the ECVFL focal length to form a minimum beam spot. Using a lens focal length control calibration table, the object feature depths are computed. Transverse measurement of the dimensions of each object feature is done using a surface-flooding technique that completely illuminates a given feature. Alternately, transverse measurements can also be made by the variable spatial sampling scan technique, where, depending upon the feature sizes, the spatial sampling spot beam size is controlled using the ECVFL. A proof-of-concept sensor is demonstrated using an optical beam from a laser source operating at a power of 10 mW and a wavelength of 633 nm. A three-dimensional (3D) test object constructed from LEGO building blocks forms has three mini-skyscraper structures labeled A, B, and C. The (x,y,z) dimensions for A, B, and C are (8 mm, 8 mm, 124.84 mm), (24.2 mm, 24.2 mm, 38.5 mm), and (15.86 mm, 15.86 mm, 86.74 mm), respectively. The smart sensor experimentally measured (x,y,z) dimensions for A, B, C are (7.95 mm, 7.95 mm, 120 mm), (24.1 mm, 24.1 mm, 37 mm), and (15.8 mm, 15.8 mm, 85 mm), respectively. The average shape sensor transverse measurement percentage errors for A, B, and C are $\pm 0.625\%$, $\pm 0.41\%$, and $\pm 0.38\%$, respectively. The average shape sensor axial measurement percentage errors for A, B, and C are $\pm 4.03\%$, $\pm 3.9\%$, and $\pm 2.01\%$, respectively. Applications for the proposed shape sensor include machine parts inspection, 3D object reconstruction, and animation

OCIS codes: 280.0280, 280.4788, 120.4820.

1. Introduction

Three-dimensional (3D) object sensing is required in a variety of industrial and scientific applications, such as thermal sensing, animation, laser machining, parts inspection, virtual reality, building scanning, and architecture and model construction. Various [1] techniques have been proposed for 3D object sensing and include using computer vision [2], wavelength scanning and selection [3–5], triangulation with multiple cameras [6–8], triangulation with structured illumination [9], optical fringe projection [10], moiré topology [11,12], optical speckle fields [13], time/frequency RF modulation of the laser beam (i.e., laser radar) [14], position sensitive detection [15], and holography [16,17]. The most direct method for target 3D information measurement involves a point-by-point scanning of a laser beam in the transverse dimension of the target to acquire the target transverse data, while the target axial (in the light direction) dimension data is determined by classic distance sensing methods, such as laser radar or triangulation.

Although the use of multiple wavelengths to image a 3D object is a direct approach to imaging, it has

0003-6935/10/071139-12$15.00/0

limitations, including the target's wavelength sensitive optical effects and the wideband requirements for the optical hardware requirements. Thus, an alternative approach proposed requires the use of a single-wavelength fast 3D laser scanner [18] that directly scans a 3D object, and single-point high-speed photodetection for the signal processing of received light [19]. This method also has its limitations, as it is suited for high optical quality retroreflective targets so the received laser light can be coupled back into the fiber optics or the point photodetector. Ideally, one would like to use a distance sensor that not only acquires 3D object reconstruction data noninvasively and directly from an illuminated target, but also uses efficient laser beam scanning with minimal volumetric data generation for object reconstruction and efficient received light optical detection.

Recently, an optical distance sensor using direct spatial processing has been proposed and demonstrated [20] that does not use time/frequency modulation of the light, and deploys the highest optimal spatial profiling resolution (i.e., transverse to optical beam propagation axis) at all axial distances of the 3D scan operation. This paper deploys the proposed spatial processing distance sensor in Ref. [20] such that it forms a spatially smart optical sensor to reconstruct 3D targets [21]. The paper begins with the design theory of the proposed sensor. A basic experiment is conducted to image a given 3D object, and theoretical versus experimental data are compared. The impact of the proposed sensor to data compression is also evaluated as it results in smartness of operation.

2. Proposed Agile Lens Smart Shape Sensor Design

Figure 1 shows the design for the proposed agile lens smart shape sensor. The sensor uses a laser source (LS) as an optical input to the system. The optical beam from the LS is made to pass through an electronically controlled variable focus lens (ECVFL) placed at a distance L_1 from the exit aperture of the LS. An ECVFL can be designed using several device technologies, such as optofluidics, liquid crystals, deformable mirrors, and microelectromechanical systems (MEMS). For example, the focal length F of the ECVFL can be tuned by the change of the applied voltage V to the lens. The Gaussian beam from the LS expands to a $1/e^2$ radius of H at the ECVFL plane with the beam divergence angle θ. The degree of convergence or divergence of the optical beam after passing through the ECVFL depends upon the focal length F to which it is tuned. After passing through the ECVFL, the beam is made to fall over the surface of the object, the shape of which has to be determined. To accurately determine a given object shape, both the axial and transverse dimensions of the object have to be ascertained. The next section

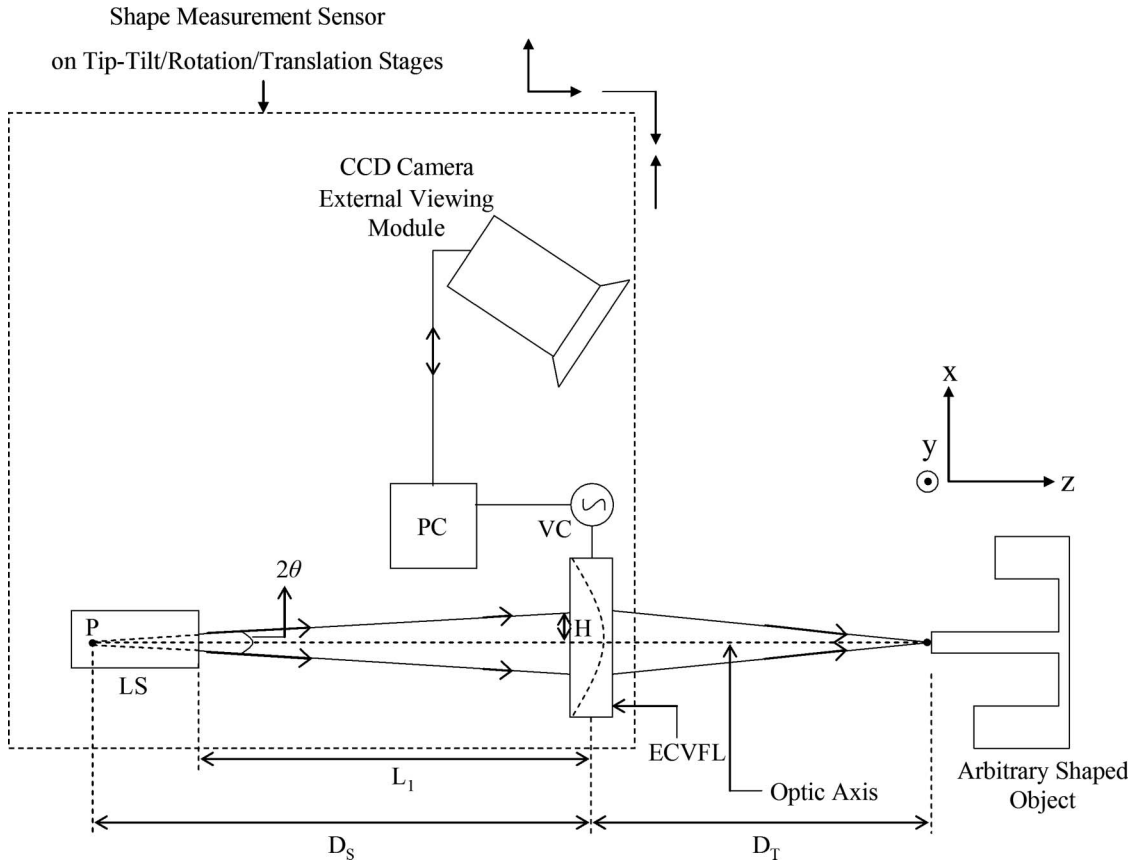

Fig. 1. Proposed smart agile remote optical sensor for 3D object shape measurements. Spherical lens, S1; laser source, LS; electronically controlled variable focus lens, ECVFL; voltage controller, VC.

discusses the methods for determining the axial and transverse dimensions using the proposed sensor.

A. Three-Dimensional Object Feature Depth Measurement Technique

The proposed smart shape sensor in Fig. 1 measures the axial dimensions or depth of a given feature in an object by imaging a virtual minimum waist point P onto the surface of interest on the object. The ECVFL voltage-dependent focal length $F(V)$ is tuned such that a minimum beam spot forms over the surface of the object under examination. First, a reference surface on the object is chosen, where $D_{T\text{-REF}}$ is the distance between this surface and the ECVFL. A minimum beam spot would form on this reference plane at a unique applied voltage and focal length $F(V)$. The required focal length for minimum beam spot formation at a different D_T is determined in the following way. A virtual minimum spot point P, as shown in Fig. 1, is determined by tracing back the marginal rays coming out of the laser. The distance D_S of point P from the ECVFL plane is determined from ray trace equations as

$$D_S \approx [H/\theta]. \tag{1}$$

The best focus condition for the laser beam over a given surface at a distance D_T from the ECVFL is governed by the imaging condition with the object point taken as P. This best focus condition, depending on F, is given by

$$D_T = (D_S F)/(D_S - F). \tag{2}$$

Therefore, for every distance D_T, there will a unique F for which the best focus imaging condition holds true. The axial depths of different object features are determined by comparing the best focus conditions for each surface to the one for the reference surface. The optical beam falling over a given object surface is observed through a CCD-camera-based movable viewing module that is focused on the surface of interest. Focal length F is recorded as soon as the best focus for a given feature surface is observed on the viewing module and, using Eq. (2), D_T is determined. The procedure for axial measurements is repeated for each given surface by laterally scanning the entire object and making similar depth measurements for each feature. Different features of varying depths with respect to the reference surface require different values of F to achieve the best focus condition resulting in a unique D_T measurement for each feature on the given object. The depth of a feature D_F can then be determined as

$$D_F = |D_{T\text{–REF}} - D_T|. \tag{3}$$

The axial depth resolution depends on the smallest attainable voltage step for the ECVFL using a particular voltage controller. The derivative of D_T with respect to F is calculated from Eq. (2) and is given by

$$\frac{dD_T}{dF} = \frac{D_S^2}{(D_S - F)^2}. \tag{4}$$

Using Eq. (4), the depth resolution step is calculated as

$$\Delta D_T(V) \approx \frac{dD_T}{dF}\Delta F(V) = \frac{D_S^2}{(D_S - F)^2}\Delta F(V). \tag{5}$$

The focal length step ΔF depends upon the regime of operation of the ECVFL. The variation of F with applied voltage V for the ECVFL can be nonlinear and, therefore, ΔF is a function of V. The dynamic range of the shape sensor depth measurement depends upon the range of focal lengths at which the ECVFL can operate and the degree of collimation of the input optical beam. A higher beam collimation results in a higher dynamic range of operation for feature depth measurements. Substituting Eq. (1) into Eq. (2), one gets

$$D_T = \frac{H \times F}{(H - F\theta)}. \tag{6}$$

Hence, the D_T measurement range depends on the degree of collimation θ of the laser beam and the ECVFL maximum focal length F_{Max} and minimum focal length F_{Min}. Thus, the dynamic range R_1 for depth measurement is given as

$$\begin{aligned} R_1 &= D_{T\text{–Max}} - D_{T\text{–Min}} \\ &= H\left(\frac{F_{\text{Max}}}{(H - F_{\text{Max}}\theta)} - \frac{F_{\text{Min}}}{(H - F_{\text{Min}}\theta)}\right). \end{aligned} \tag{7}$$

F_{Max} and F_{Min} depend on the specific ECVFL design and its fabrication. The larger the range of the ECVFL focal lengths, the higher is the dynamic range of operation for depth measurements. The degree of collimation also determines the dynamic range R_1 and it can be adjusted when detecting feature depths in objects with various depth levels for different applications.

The percentage resolution R_δ of the feature depth measurement is given by

$$R_\delta = \frac{\Delta D_T}{D_T} = \frac{(D_S - F)D_S + D_S F}{(D_S - F)^2} \times \Delta F \times \frac{D_S - F}{D_S F}, \tag{8}$$

$$\begin{aligned} \Rightarrow R_\delta &= \frac{\Delta D_T}{D_T} = \frac{(D_S - F)D_S + D_S F}{(D_S - F)D_S F} \times \Delta F \\ &= \left(\frac{1}{F} + \frac{1}{D_S - F}\right)\Delta F. \end{aligned} \tag{9}$$

As seen from Eq. (9), the percentage resolution mathematically depends upon the laser beam collimation because $D_S \approx [H/\theta]$, the focal length F to which the

ECVFL is tuned, and the minimum focal length step ΔF that can be made given a specific ECVFL type and its controller. From a physical and experimental point of view, the resolution also depends on the CCD camera pixel size as well as the optical wavefront spoiling effects caused by the camera lens, such as the effect of imaging lens spherical aberrations.

B. Three-Dimensional Object Feature Transverse Measurement Technique

Subsection 2.A explained how the axial depth measurements are made for any feature on the 3D test object. To accurately determine the shape of a test object, the transverse dimensions of each feature also need to be determined, along with the axial depth measurements. The proposed sensor uses two transverse dimension measurement approaches that are either deployed individually or simultaneously.

1. *Optical Beam Flooding Technique*

If the feature size is such that $\Delta x < w_{T\text{-Max}}$ and $\Delta y < w_{T\text{-Max}}$, an optical flooding technique is used by the sensor. Here, $w_{T\text{-Max}}$ is the maximum null-to-null optical beam size for a given D_T that occurs when the ECVFL focal length is at its maximum of F_{Max}. In this defined target flooding method, the optical beam falling on a given uniform (i.e., same axial depth) surface is made to expand over that surface by controlling the ECVFL applied voltage. Thus, the expanded beam that falls on the flat object feature surface completely covers this surface with the illuminating light. As a result of surface scattering, a flat feature outline is produced that can be clearly seen by a target viewing CCD camera. Note that any part of the beam not falling over the feature surface does not get highly scattered from the same axial plane, thus marking an outline of the object feature. Also note that the level of surface scattering will depend on a number of optical and target material parameters, such as incidence angle, light polarization, light wavelength, target material surface roughness scale, and target material optical absorption and reflectance values.

2. *Variable Sampling and Scanning Technique*

The second method for transverse shape measurement is the more traditional beam scan method and it is used when a target surface has $\Delta x, \Delta y > w_{T\text{-Max}}$ dimensions. In this case, the shape sensor module is translated in the x and y directions to enable the smart illuminating laser beam to scan a given surface in the target x–y plane. Using the proposed sensor design, the spatial sampling resolution of the scan can be adjusted by tuning the ECVFL. This aspect is further elaborated in Section 4. The beam scanning is stopped as soon as the optical beam starts getting clipped at any edge of the surface under test. The sensor module motion is accurately recorded to enable measurement of the transverse dimensions of a given illuminated surface. This defined procedure is repeated for all 3D object surfaces to determine the complete 3D view of the sample object. The next section explains the sensor beam physics used to determine the transverse dimensions of the 3D object via the flooding and the beam scan techniques.

C. Sensor Beam Physics for the Beam Scan and Beam Flooding Techniques

A Gaussian beam optical field can be represented by the complex q-parameter $q(z)$ [22] such that

$$E(r,z) \propto \exp(jkr^2/2q(z)), \tag{10}$$

where

$$\frac{1}{q(z)} = \frac{1}{R(z)} - j\frac{\lambda}{\pi w^2(z)}. \tag{11}$$

Here, λ is the wavelength, $R(z)$ is the radius of curvature of the beam wavefront, $k = 2\pi/\lambda$, and $r = \sqrt{x^2 + y^2}$, where (x,y) are the Cartesian coordinates of the optical field plane. $w(z)$ denotes the $1/e^2$ beam waist at any distance z from the minimum waist virtual point P. At P, substituting $R = \infty$ into Eq. (11) gives the beam q-parameter q_p as $q_P = \frac{\pi w_0^2}{\lambda} j$.

The $1/e^2$ optical beam radius at a distance D_S from point P at the liquid lens is H and the minimum beam radius at point P is w_0 with

$$H^2 = w_0^2\left(1 + \frac{\lambda^2 D_S^2}{\pi^2 w_0^4}\right), \tag{13}$$

and by solving for w_0, one gets

$$w_0 = \sqrt{\frac{H^2 - \sqrt{H^4 - \frac{4\lambda^2 D_S^2}{\pi^2}}}{2}}. \tag{14}$$

As seen in Fig. 1, the test surface of the object under measurement is located at a distance $D_S + D_T$ away from point P. The $ABCD$ matrix for beam propagation from point P to object surface plane is [22]

$$\begin{bmatrix} A & B \\ C & D \end{bmatrix} = \begin{bmatrix} 1 & D_T \\ 0 & 1 \end{bmatrix} \times \begin{bmatrix} 1 & 0 \\ -\frac{1}{F} & 1 \end{bmatrix} \times \begin{bmatrix} 1 & D_S \\ 0 & 1 \end{bmatrix}, \tag{15}$$

$$\Rightarrow \begin{bmatrix} A & B \\ C & D \end{bmatrix} = \begin{bmatrix} 1 - \frac{D_T}{F} & D_S + D_T - \frac{D_S D_T}{F} \\ -\frac{1}{F} & 1 - \frac{D_S}{F} \end{bmatrix}. \tag{16}$$

From Eq. (16), it is determined that

$$A = 1 - \frac{D_T}{F}, \tag{17}$$

$$B = D_S + D_T - \frac{D_S D_T}{F}, \tag{18}$$

$$C = -\frac{1}{F}, \tag{19}$$

$$D = 1 - \frac{D_S}{F}. \tag{20}$$

The complex q-parameter q_T at the plane of interest of the test object is given by

$$q_T = \frac{Aq_P + B}{Cq_P + D}, \tag{21}$$

$$q_T = \frac{Aq_P + B}{Cq_P + D} \Rightarrow 1/q_T = \frac{Cq_P + D}{Aq_P + B}. \tag{22}$$

From Eq. (11),

$$\mathrm{Im}(1/q_T) = \frac{-\lambda}{\pi w_T^2} = \mathrm{Im}\left(\frac{Cq_P + D}{Aq_P + B}\right), \tag{23}$$

$$\Rightarrow w_T = \sqrt{\frac{-\lambda}{\pi \times \mathrm{Im}\left(\frac{Cq_P+D}{Aq_P+B}\right)}}. \tag{24}$$

From Eq. (24), the optical beam $1/e^2$ spot size w_T falling on the surface of a given object is determined. Im denotes the imaginary part of a given quantity. The null-to-null spot size is determined using the standard Gaussian approximation, which relates the $1/e^2$ radius of a Gaussian beam to a beam radius that contains approximately 99% of optical power. Thus, one can write [23]

$$R_{99} = 1.517 R_{1/e^2}. \tag{25}$$

Here, R_{99} is the beam radius that contains 99% of the total beam power and R_{1/e^2} is the $1/e^2$ beam radius. It is seen from Eq. (24) that the beam radius w_T depends on the beam $ABCD$ parameters, which depend on the focal length of the ECVFL. By changing F, the beam size w_T can be varied from a minimum to a maximum at the object surface plane. The ability to alter the size of the optical beam falling on a given surface using the ECVFL enables the sensor to work in transverse scan mode with a variable scan resolution. Depending on the transverse dimension of a given feature on an object, the scan resolution can be adjusted. This is a highly desirable feature, as redundant scan points are avoided for object features with large transverse dimensions or large flat objects with slowly changing surface features over the object structure.

The transverse resolution and the transverse dynamic range of the sensor measurement are critical in the proposed sensor operation. The transverse resolution is calculated in the following way. We know from Eq. (5) that the axial resolution is given by

$$\Delta D_T(V) = \frac{D_S^2}{(D_S - F)^2} \Delta F(V). \tag{26}$$

The smallest beam spot forms at a given D_T for an ECVFL focal length F. When the applied voltage is changed by the smallest voltage step ΔV without changing the object surface distance, the new best focus distance $D_{T\text{-New}}$ is given by

$$D_{T\text{–New}} = D_T + \Delta D_T, \tag{27}$$

and the new focal length is given by

$$F_{\mathrm{New}} = F + \Delta F. \tag{28}$$

From Eq. (16), the new $ABCD$ parameters for the beam with object plane D_T from the ECVFL would be given by

$$A_{\mathrm{New}} = 1 - \frac{D_T}{F_{\mathrm{New}}}, \tag{29}$$

$$B_{\mathrm{New}} = D_S + D_T - \frac{D_S D_T}{F_{\mathrm{New}}}, \tag{30}$$

$$C_{\mathrm{New}} = -\frac{1}{F_{\mathrm{New}}}, \tag{31}$$

$$D_{\mathrm{New}} = 1 - \frac{D_S}{F_{\mathrm{New}}}. \tag{32}$$

The subscript "New" denotes the slightly modified $ABCD$ parameters at F_{New}. The complex q-parameter at this slightly new focal length is q_{new}, and it is given by

$$q_{\mathrm{New}} = \frac{A_{\mathrm{New}} q_P + B_{\mathrm{New}}}{C_{\mathrm{New}} q_P + D_{\mathrm{New}}} \Rightarrow 1/q_{\mathrm{New}} = \frac{C_{\mathrm{New}} q_P + D_{\mathrm{New}}}{A_{\mathrm{New}} q_P + B_{\mathrm{New}}}. \tag{33}$$

The beam waist at this new location is w_{New}, and it is given by

$$w_{\mathrm{New}} = \sqrt{\frac{-\lambda}{\pi \times \mathrm{Im}(1/q_{\mathrm{New}})}} = \sqrt{\frac{-\lambda}{\pi \times \mathrm{Im}\left(\frac{C_{\mathrm{New}} q_P + D_{\mathrm{New}}}{A_{\mathrm{New}} q_P + B_{\mathrm{New}}}\right)}}. \tag{34}$$

The transverse resolution R_T is calculated by the change of the beam radius at a fixed plane D_T from the ECVFL when the control voltage is stepped up by ΔV, and it is given by

$$R_T = |w_{\mathrm{New}} - w_T|, \tag{35}$$

where

$$R_T = \left| \sqrt{\frac{\lambda}{\pi}} \times \left(\sqrt{\frac{-1}{\mathrm{Im}\left(\frac{C_{\mathrm{New}} q_P + D_{\mathrm{New}}}{A_{\mathrm{New}} q_P + B_{\mathrm{New}}}\right)}} - \sqrt{\frac{-1}{\mathrm{Im}\left(\frac{C q_P + D}{A q_P + B}\right)}} \right) \right|. \tag{36}$$

The factor by which the spatial sampling can be altered depends on the difference between the minimum and the maximum spot sizes for a given D_T. This, in turn, depends on the range of focal lengths at which one can tune the ECVFL. The maximum-to-minimum spatial sampling factor ξ is defined as

$$\xi = \frac{w_{T-\mathrm{Max}}}{w_{T-\mathrm{Min}}}. \tag{37}$$

ξ can be computed for each D_T by tuning the ECVFL for all permissible values of F. To determine the spatial sampling resolution of the shape sensor, the feature size that the sensor is trying to determine has to be taken into account. In case the beam flooding technique is not used, then the scan technique should be able to determine the transverse dimensions of the smallest feature. The choice of the technique for transverse measurement depends on the feature size to be measured as well as the type of target and its application scenario.

3. Three-Dimensional Shape Sensing Experiment

The setup in Fig. 1 was implemented using an electrowetting-technology-based [24] Arctic 320 tunable focus liquid lens [25]. The focal length of this lens varies from $F_{\mathrm{Min}} = 4.89\,\mathrm{cm}$ ($V = 58\,\mathrm{V}$) to $F_{\mathrm{Max}} = 21.28\,\mathrm{cm}$ ($V = 43\,\mathrm{V}$) when used in a convex lensing arrangement. In the concave lensing configuration, the focal length varies from a near flat state to $-19.9\,\mathrm{cm}$. The laser source used for the experiment is a 633 nm He–Ne laser with a beam divergence angle θ of 1.24 mrad. The beam expands to a diameter of $2H = 0.655\,\mathrm{mm}$ at the ECVFL plane for $L_1 = 12\,\mathrm{cm}$. Given these conditions and using Eq. (1), one computes $D_S = 26.43\,\mathrm{cm}$. This optical beam from the laser source passes through the ECVFL and hits the object whose shape is to be determined. The test object was constructed using LEGO blocks and it is shown in Fig. 2. The test object was carefully designed such that different protrusions would have distinguishable dimensions in length, width, and height with respect to a reference measurement plane. Figure 2(b) shows the dimensions of this test object showing three different protrusions. These reference measurements were made using a caliper.

In Fig. 3, calibration curves for the demonstrated sensor are plotted. Three sets of theoretical and experimental curves are shown. Figure 3(a) shows the variation of the applied voltage V required to form a minimum beam spot at different object distances D_T.

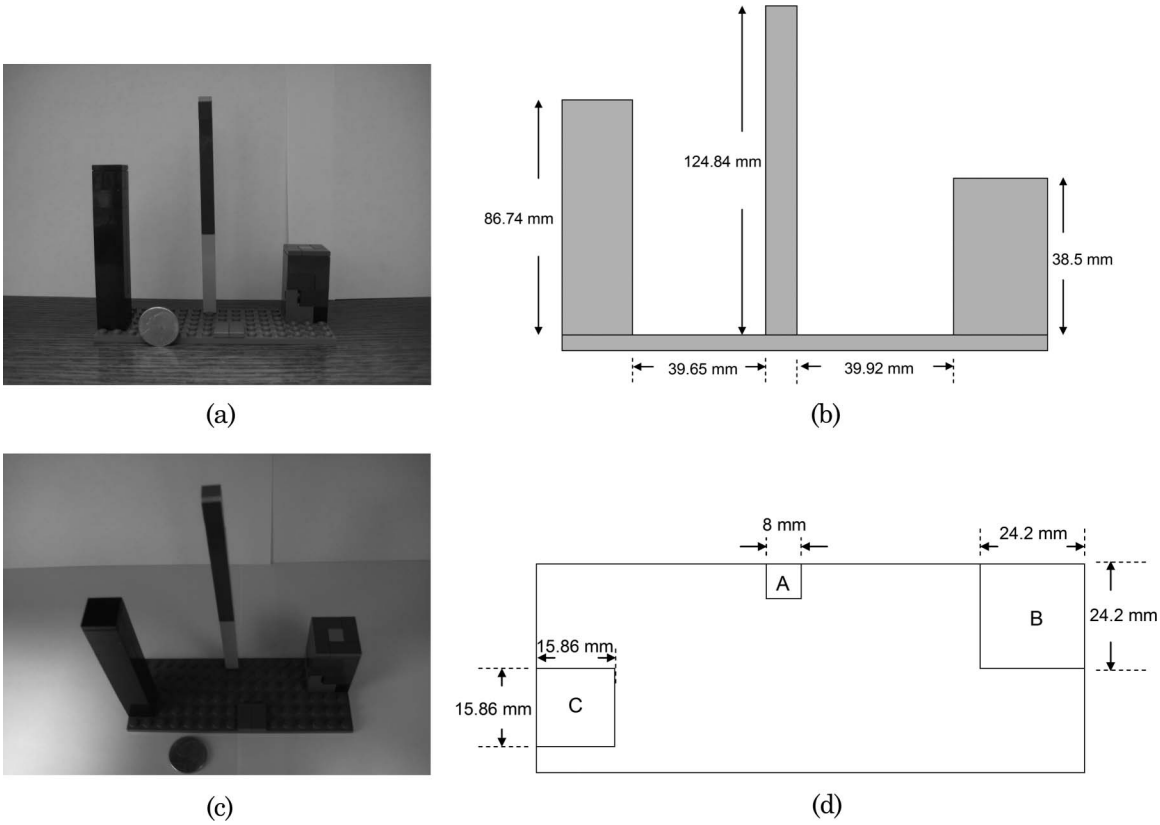

Fig. 2. The skyscraper structures test object: (a) top view photograph, (b) top view drawing, (c) side view photograph, and (d) side view drawing. A U.S. currency nickel (5 cents) coin is shown for scale comparison.

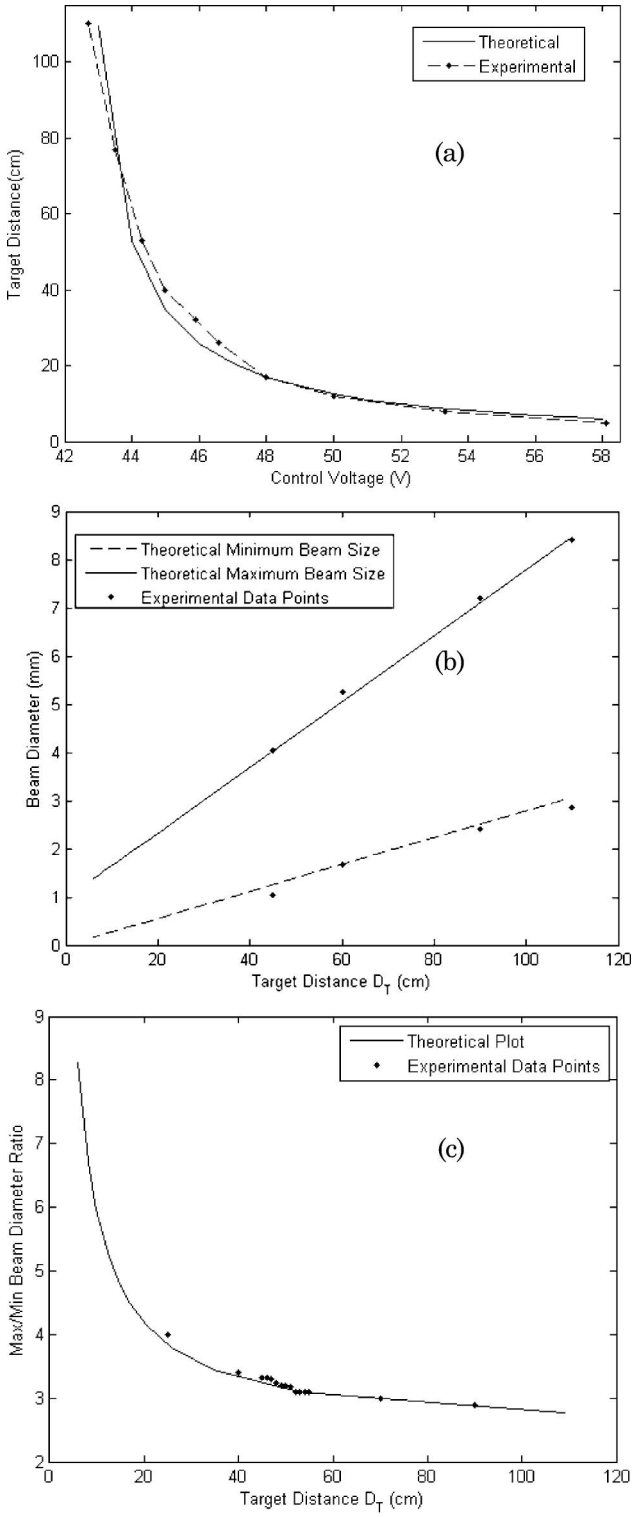

Fig. 3. Sensor calibration plots for (a) target distance versus applied voltage for minimum spot size, (b) minimum and maximum spot diameters for different target ranges, and (c) spot size dynamic range for different target distances.

The theoretical curve in Fig. 3(a) is plotted using Eqs. (1)–(6). This plot is used to measure the depths of different planes for a 3D object. Next, in Fig. 3(b), the minimum and maximum $1/e^2$ beam spot diameters for different object plane distances have been plotted. This spot size variation is determined by the tuning range of the ECVFL focal length. The minimum spot size at a particular D_T determines the highest spatial sampling rate and, hence, the smallest feature that can be accurately determined. The maximum beam size determines the lowest spatial sampling possible with the proposed shape sensor and it is an extremely useful characteristic when probing larger surfaces with large features. The theoretical reference curve in Fig. 3(b) is plotted using Eqs. (10)–(24). Using the minimum and maximum beam spot sizes in Fig. 3(b), the ratio of the minimum-to-maximum spot sizes at different target distances is plotted in Fig. 3(c). This determines the factor by which the spatial sampling rate can be altered at different scan depths. This beam size dynamic range is found to be greater than 3 for the entire range of operation of the sensor.

For the experiment, D_T was set to be 50 cm. This is the distance from the ECVFL plane to the reference plane of the object. Feature extraction using the beam expansion flooding technique is demonstrated for surface A in Fig. 4. Three snapshots are presented as the incoming beam hitting surface A is expanded by changing V for the ECVFL from 15 to −19.9 cm. The beam is shown to expand from a null-to-null diameter of 3 mm in Fig. 4(a) to 7 mm in Fig. 4(b). Finally, the beam is expanded to cover surface A completely, as seen in Fig. 4(c), so that the feature outline is fully visible. Next, in Fig. 5, measurements made on surface B are demonstrated using the variable sampling and scanning technique, as this surface is too large to be measurable simply by using the flooding technique. As can be seen in Figs. 5(a)–5(d), the optical beam, expanded to a null-to-null diameter of 6 mm, scans surface B and is shown to touch the four corners of the surface under measurement. The beam was moved by 18.1 cm from one edge to the opposite edge. Adding up the beam diameter to this scan distance determined the dimension of surface B as 18.1 mm + 6 mm = 24.1 mm in both directions. The beam expansion method reduces the spatial sampling required to completely scan the surface. Using the same beam expansion and scan technique, the dimensions of surface C are determined to be 15.8 mm × 15.8 mm. These measured dimensions are marked in Fig. 6.

The height of each protrusion is measured by making the optical beam fall over each surface one at a time and forming a minimum spot over each surface, and the distance of the surface from the ECVFL plane is determined. The distance $D_{T\text{-REF}}$ of the reference plane of the test object from the ECVFL is also determined in the same way. The minimum spot at the reference plane forms at an applied voltage of 44 V. Hence, from Fig. 3(a), D_T is determined to be 50 cm. The minimum beam spots for surface A, surface B, and surface C are formed for applied voltages of 44.3, 44.9, and 44.5 V, respectively. The distances of surface A, surface B, and surface C from the

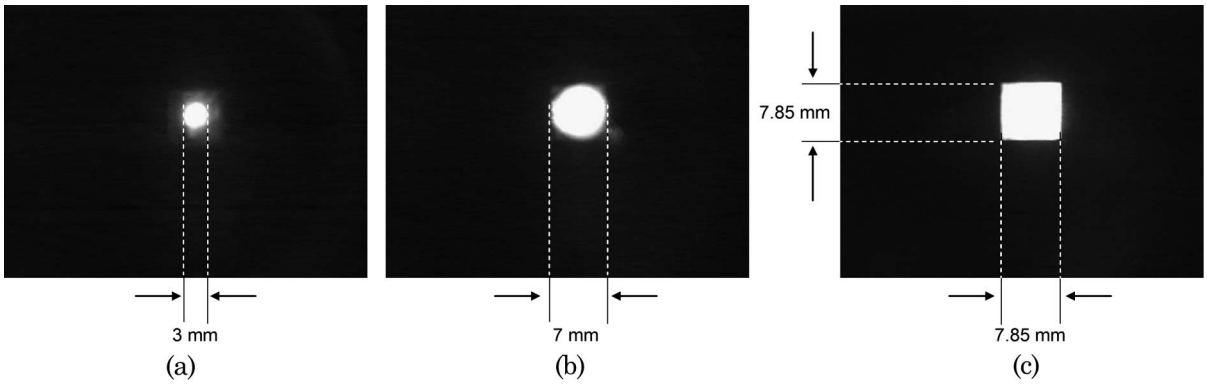

Fig. 4. Mini skyscraper structures feature extraction of surface A using the flooding method implemented by agile-lensing-based beam expansion when surface A is 37.5 cm from the ECVFL.

ECVFL plane are thus determined to be 46.3, 38, and 41.5 cm, respectively. Using Eq. (2), surface A is measured to be 3.7 cm in height, surface B is 12 cm in height, and surface C is 8.5 cm in height with respect to the reference plane.

The CCD camera imaging system has a magnification ratio M. To accurately determine the transverse dimensions of each target feature, M has to be determined. This image capture calibration is done by measuring the minimum beam diameter as seen by the CCD camera for a given D_T and comparing it to the expected minimum beam size for that value of D_T. The spot size (also captured on the CCD camera) at this given D_T is varied until such a beam spot is achieved that increasing or decreasing the ECVFL applied voltage by one step ΔV only results in an increase in the spot size. This signifies the beam spot size minima, and the corresponding optical beam is mapped to a certain number of pixels on the CCD camera. The size of the CCD pixel grid and the number of grid elements are already known. Using this information, the beam spot size on the CCD is determined. The theoretical minimum beam spot size for any given D_T is determined using Eq. (24). M is determined for a given D_T by comparing the minimum beam size measured by the CCD to the theoretical minimum beam size. Once M is determined, the viewing module focus is fixed for small 3D objects

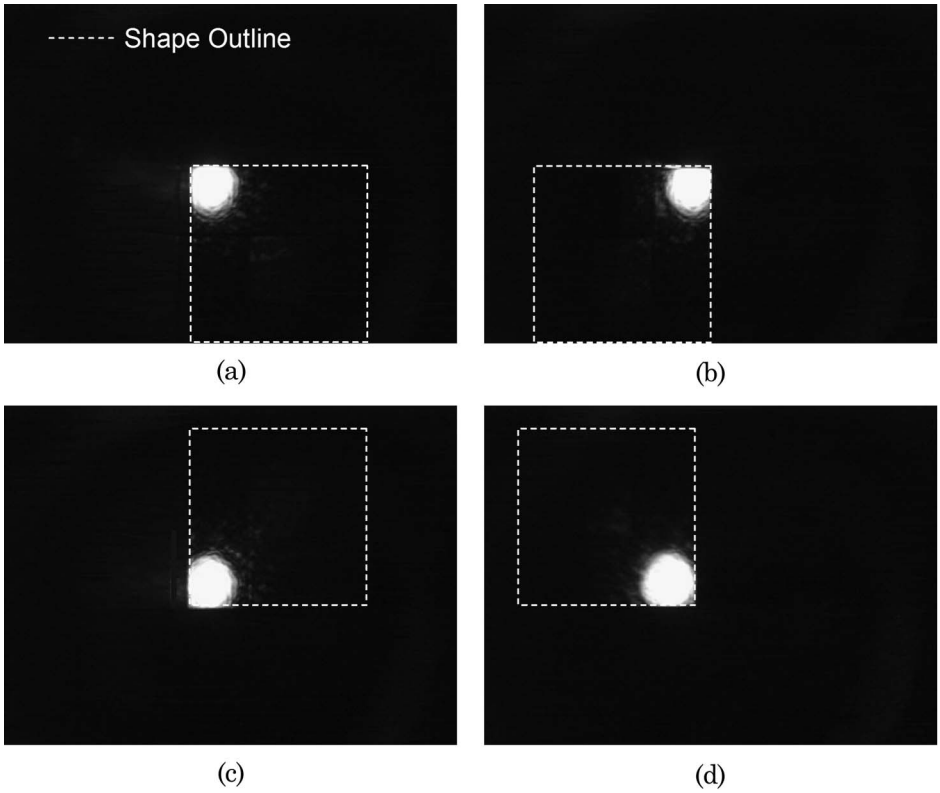

Fig. 5. Mini skyscraper structures feature extraction of surface B using an expanded beam of null-to-null diameter of 6 mm and employing low-resolution surface scanning by object motion.

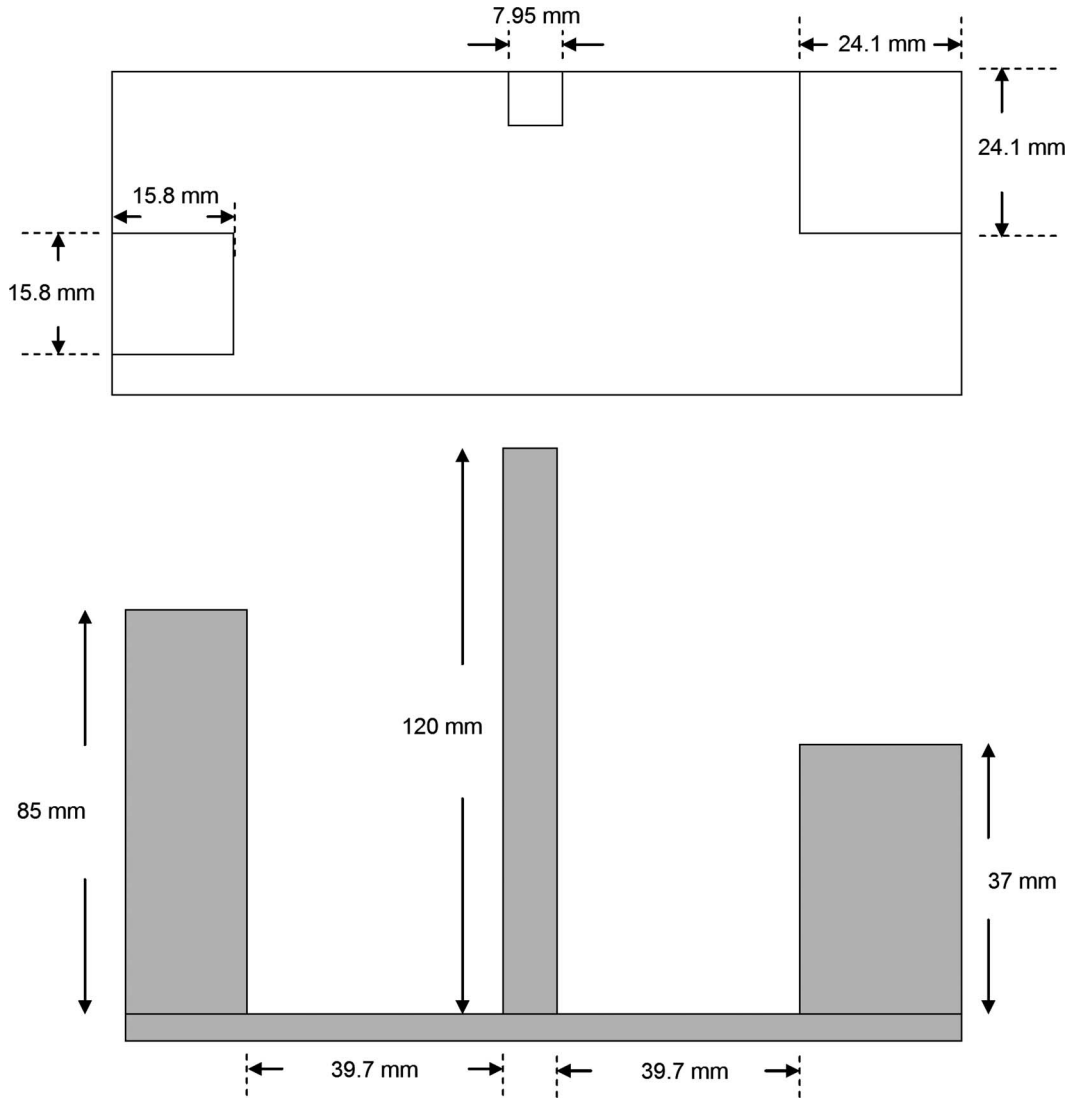

Fig. 6. Reconstructed shape of the mini skyscraper structures 3D test using both the flooding and the scanning techniques.

that require a small range of viewing module foci. For large objects, the viewing module focus has to be altered and M is determined for each surface feature. M is measured to be 0.182 for the experiment. Using Eq. (7), the axial resolution of the sensor is determined to be <1.7 cm. Similarly, using Eq. (36), the transverse resolution of the sensor is calculated to be <0.15 mm.

Figure 7 shows the block diagram for the computer algorithm used to compute the null-to-null beam diameter of a given CCD image. After reading the gray-scale x–y image from the CCD, the maximum pixel intensity value Ψ is stored for reference. Next, the image is scanned line by line in both the x direction and the y direction. As one determines the null-to-null beam size according to the definition of Eq. (25),

for each line scan the maximum number of consecutive pixels having an intensity $> 0.01\Psi$ is recorded. Then the longest pixel sequence in both the x direction ($P_{X\text{-Max}}$) and the y direction ($P_{Y\text{-Max}}$) is computed. Next, the null-to-null beam diameter in both the x and y directions is computed by the following equations:

$$2W_{T\text{-}X} = P_{X\text{-Max}} \times D_{X\text{-Pixel}}, \tag{38}$$

$$2W_{T\text{-}Y} = P_{Y\text{-Max}} \times D_{Y\text{-Pixel}}, \tag{39}$$

where $D_{X\text{-Pixel}}$ and $D_{Y\text{-Pixel}}$ are the CCD pixel pitch values in the x direction and the y direction, respectively.

The dynamic range R of feature height measurement is 109.44 cm. This dynamic range is determined by the range of focal lengths for which the ECVFL can be tuned. The percentage errors in transverse measurements for surface A, surface B, and surface C are 0.625%, 0.41%, and 0.38%, respectively. Similarly the height measurement errors for surface A, surface B, and surface C are 4.03%, 3.9%, and

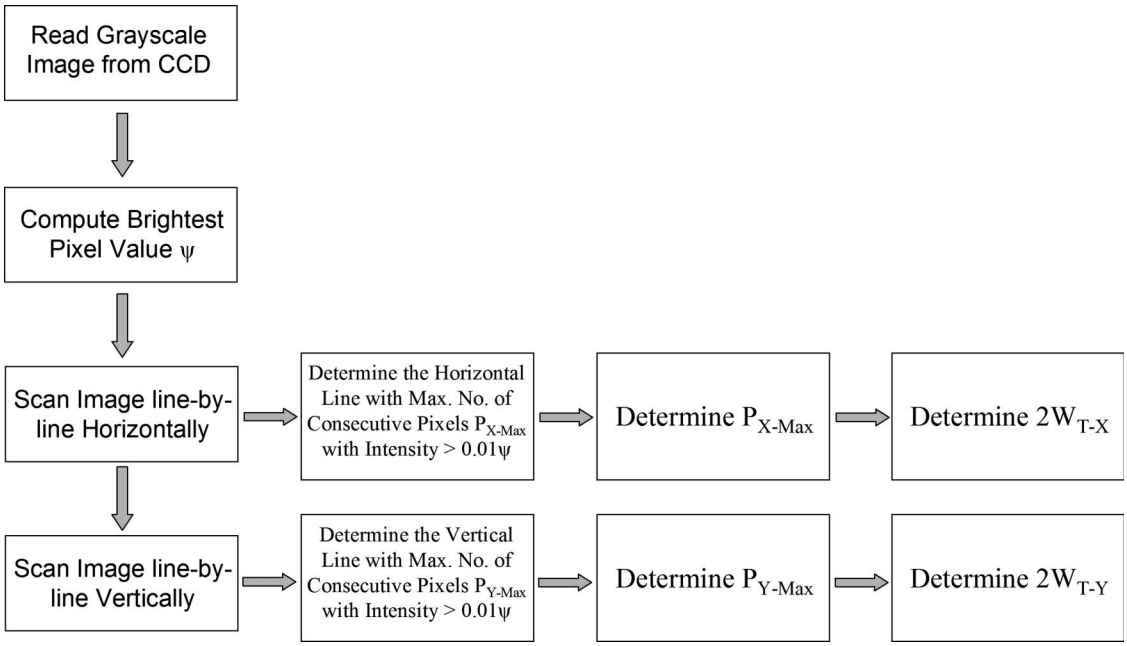

Fig. 7. Block diagram of the computer algorithm used to determine beam diameters.

2.01%, respectively. A higher dynamic range for height measurement can be achieved for the proposed sensor if the laser beam is collimated instead of being used as a raw beam, as has been done for the present experimental demonstration.

The Gaussian laser beam has a $\lambda/4$ Rayleigh-criterion-based focal depth of $\Delta z \sim \pm 2\lambda(f\#)^2$, where λ is the wavelength of the optical beam and $f\#$ (f-number) of the ECVFL is given by $F(V)/D$ where D is the diameter of the clear aperture of the ECVFL. This focal depth Δz is $<0.492\,\text{cm}$ for the operating range of the demonstrated sensor using an ECVFL with $D = 0.34\,\text{cm}$ and $F(V) = F_{\text{Max}} = 21.28\,\text{cm}$. Much like a confocal microscope, the depth of focus sets the fundamental limitation on the depth resolution of the proposed sensor.

4. Implications for Three-Dimensional Information Capture and Transfer

As shown in Fig. 8, the proposed smart spatial sampling optical sensor for 3D targets can match the transverse optical beam size to the target transverse feature size at the given axial (along the optical axis) location. This can be done by engaging the diverging beam or negative focal length control of a given ECVFL lens. Hence, spatial sampling smartness is produced with instantaneous spatial mapping of the flat target feature zone (e.g., AB, CD, and EF shown in Fig. 8) implemented without the need for point-by-point smallest resolution transverse beam scanning over the flat feature zone. Thus, compared to prior-art optical distance measurement 3D sensors [see Figs. 8(a) and 8(b)] where the scanning beam spot size stays fixed (apart from the natural beam diffraction-based expansion) for all 3D scan positions of the beam on the 3D target (what is called non-smart spatial sampling), the proposed sensor adjusts the transverse beam spot size at each axial position based on the specific target's 3D shape profile [See Fig. 8(c) where the feature size is AB]. Hence, the agile sampling spot can be several times the spot size due to a naturally divergent beam. Of course, for higher spatial sampling resolution in the transverse plane, the proposed sensor operation can be used with the ECVFL in its converging lens state [see Fig. 8(d)]. Thus, using the ECVFL diverging state, an optimized smaller sampling dataset (see Fig. 9) can be generated for a given target, in particular when the feature size is smaller (e.g., CD or EF in Fig. 8) than the natural diffracted beam spot size [Fig. 8(a)]. Figure 9 assumes a symmetric sample target feature and the proposed sensor is engaging the diverging power of the ECVFL lens, i.e., $F(V)$ is negative. Specifically, one can define a transverse feature scan data compression factor as

$$C_F = \left(\frac{N}{N_C}\right)^2, \tag{40}$$

$$\Rightarrow C_F = \left(\frac{w_{T\text{-Div}}}{w_{T\text{-}\infty}}\right)^2, \tag{41}$$

where N_C is the compressed number of scan pixels in the x or the y direction and N is the number of uncompressed pixels for the same scan length. Here, $w_{T\text{-}\infty}$ and $w_{T\text{-Div}}$ are the beam radii for the classic diffraction case (when no agile lens is used) and the scenario with an activated agile lens, respectively. Given a situation where $w_{T\text{-Div}} = 5w_{T\text{-}\infty}$, the compression factor $C_F = 25$, implying 25 times less data generated for storage and transfer. In addition, 25 times smaller

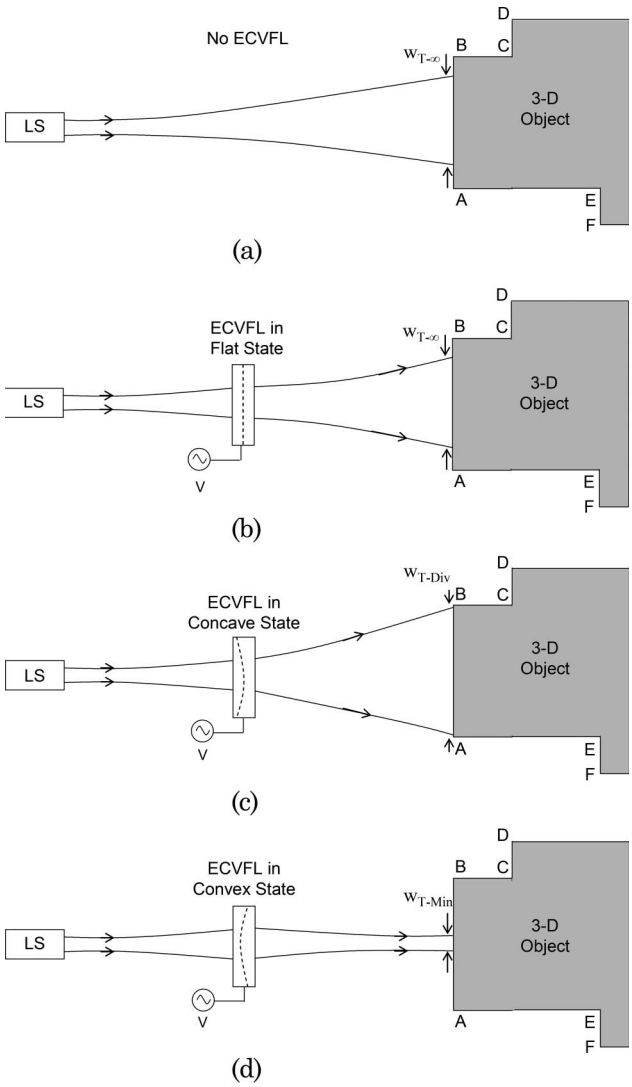

Fig. 8. Transverse direction 3D object spatial sampling by a scanning laser beam using (a) the classic uncompressed data diffraction limited beam expanding laser spot, (b) a method similar to classic unassisted laser beam scanning when ECVFL is in its flat no-lensing state, (c) smart data-compressed large beam spot size scanning using the ECVFL in its diverging lens mode with spot size matched to target feature size AB, and (d) high-spatial-resolution target feature sampling using the ECVFL in its converging lens mode with laser spot smaller than target feature size.

object scanning operations are needed, which could imply faster feature scan completion time.

Depending on the optical surface quality of the target (diffused or specular), the targeted beam spot on the object is monitored by an off-axis optical camera or an on-axis photodetector optics and electronics. Thus, the spot detection optics and electronics provides feedback to the variable lens controllers to produce the minimal scanned spot beam to gather the shape reconstruction data for the 3D object. Hence, the proposed novel sensor using agile focal lengths allows volumetric data compression for transverse measurements during the remote sensing of 3D objects.

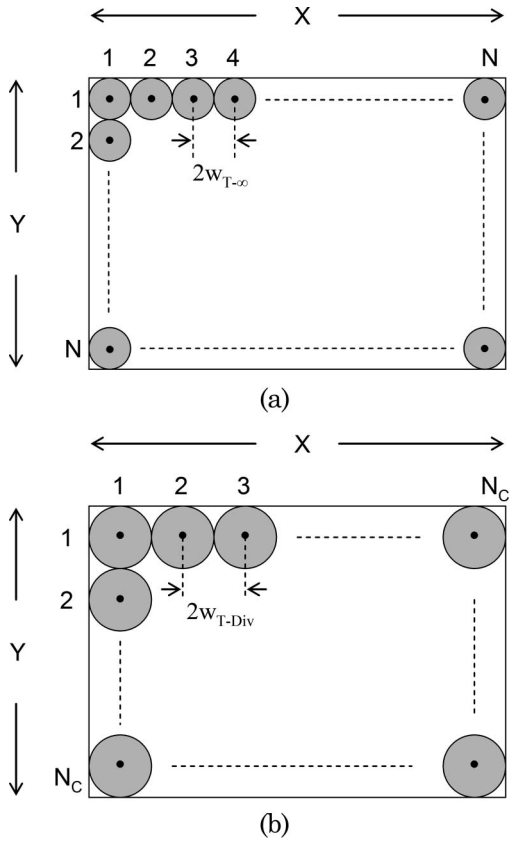

Fig. 9. (a) Fixed laser spot size transverse beam scanned uncompressed target feature mapping and (b) agile lens smart laser beam spot size transverse beam scanned compressed data target feature mapping.

5. Conclusion

This paper presents a novel agile lensing-based technique to measure the shape of a given 3D object. Specifically, the depth measurement for the 3D object is made by focusing an optical beam on the surface of each feature. The focal length to which the agile lens is tuned determines the depth of each feature. The transverse measurements are made using a proposed optical beam flooding technique or the more traditional optical beam scan technique. A proof-of-concept sensor is designed for laboratory experimentation and successfully demonstrated to measure the 3D shape of three given mini-skyscraper structures. The proposed sensor can be particularly useful for industrial applications where remote measurements of well-structured 3D objects are required, such as in extreme environments of highly corrosive chemicals, hot/cold temperatures, and high electric/magnetic fields.

The authors thank Nuonics, Inc. for equipment support and Dr. Frank Perez for his original technical insights. The authors also thank Mehdi Riza and Shems Riza for the LEGO mini-skyscraper 3D test object.

References

1. F. Chen, G. M. Brown, and M. Song, "Overview of three-dimensional shape measurement using optical methods," Opt. Eng. **39**, 10–22 (2000).

2. P. J. Besl, "Active optical range imaging sensors," in *Machine Vision and Applications* (Springer, 1988), Vol. 1, pp. 127–152.
3. H. J. Tiziani and H. M. Uhde, "Three-dimensional image sensing by chromatic confocal microscopy," Appl. Opt. **33**, 1838–1843 (1994).
4. N. A. Riza and Y. Huang, "High speed optical scanner for multi-dimensional beam pointing and acquisition," in *Lasers and Electro-Optics Society 12th Annual Conference Proceedings*, L. Goldberg, ed. (IEEE, 1999), pp. 184–185.
5. N. A. Riza, "Multiplexed optical scanner technology," U.S. patent 6,687,036 (3 Feb. 2004).
6. S. D. Cochran and G. Medioni, "3-D surface description from binocular stereo,"IEEE Trans. Pattern Anal. Machine Intell. **14**, 981–994 (1992).
7. G. Häusler and D. Ritter, "Parallel three-dimensional sensing by color-coded triangulation," Appl. Opt. **32**, 7164–7169 (1993).
8. K. D. Moore, "Intercalibration method for underwater three-dimensional mapping laser line scan systems," Appl. Opt. **40**, 5991–6004 (2001).
9. X. X. Cheng, X. Y. Su, and L. R. Guo, "Automated measurement method for 360° profilometry of 3-D diffuse objects," Appl. Opt. **30**, 1274–1278 (1991).
10. C. Reich, R. Ritter, and J. Thesing, "3-D shape measurement of complex objects by combining photogrammetry and fringe projection," Opt. Eng. **39**, 224–231 (2000).
11. H. Takasaki, "Moiré topology," Appl. Opt. **9**, 1467–1472 (1970).
12. S. Wei, S. Wu, I. Kao, and F. P Chiang, "Measurement of wafer surface using shadow moiré technique with Talbot effect," J. Electron. Packag. **120**, 166–170 (1998).
13. A. Anand, V. Chhaniwal, P. Almoro, G. Pedrini, and W. Osten, "Shape and deformation measurements of 3D objects using volume speckle field and phase retrieval," Opt. Lett. **34**, 1522–1523 (2009).
14. Leica Geosystems HDS 3000 3-D Laser Scanner System 2009 Data Sheet.
15. A. J. Makynen, J. T. Kostamovaara, and R. A. Myllyla, "A high-resolution lateral displacement sensing method using active illumination of a cooperative target and a focused four-quadrant position-sensitive detector," IEEE Trans. Instrum. Meas. **44**, 46–52 (1995).
16. B. Nilsson and T. E. Carlsson, "Direct three-dimensional shape measurement by digital light-in-flight holography," Appl. Opt. **37**, 7954–7959 (1998).
17. C. Wagner, W. Osten, and S. Seebacher, "Direct shape measurement by digital wavefront reconstruction and multiwavelength contouring," Opt. Eng. **39**, 79–85 (2000).
18. N. A. Riza, "Digital control polarization-based optical scanner," U.S. patent 6,031,658 (29 Feb. 2000).
19. S. A. Khan and N. A. Riza, "Confocal microscopy based agile optical endoscope using liquid crystals," in *IEEE LEOS Biophotonics Summer Topical Meeting Digest* (IEEE, 2004), pp. 10–11.
20. N. A. Riza and S. A. Reza, "Non-contact distance sensor using spatial signal processing," Opt. Lett. **34**, 434–436 (2009).
21. N. A. Riza and F. Perez, patent pending.
22. H. Kogelnik and T. Li, "Laser beams and resonators," Appl. Opt. **5**, 1550–1567 (1966).
23. E. Friedman and J. L. Miller, *Photonics Rules of Thumb: Optics, Electro-Optics, Fiber Optics, and Lasers*, 2nd ed. (McGraw-Hill, 2004), p. 170.
24. L. Saurei, J. Peseux, F. Laune, and B. Berge, "Tunable liquid lens based on electrowetting technology: principle, properties and applications," in *10th Annual Micro-optics Conference* (Elsevier, 2004), p. E-1.
25. Model Arctic 320 liquid lens technical datasheet: optical and opto-mechanical data (Varioptic SA, 2006), pp. 1–7.